

Ultracold Atoms in 1D Optical Lattices: Mean Field, Quantum Field, Computation, and Soliton Formation

R. V. Mishmash and L. D. Carr

Department of Physics, Colorado School of Mines, Golden, CO, 80401

Abstract

In this work, we highlight the correspondence between two descriptions of a system of ultracold bosons in a one-dimensional optical lattice potential: (1) the discrete nonlinear Schrödinger equation, a discrete mean-field theory, and (2) the Bose-Hubbard Hamiltonian, a discrete quantum-field theory. The former is recovered from the latter in the limit of a product of local coherent states. Using a truncated form of these mean-field states as initial conditions, we build quantum analogs to the dark soliton solutions of the discrete nonlinear Schrödinger equation and investigate their dynamical properties in the Bose-Hubbard Hamiltonian. We also discuss specifics of the numerical methods employed for both our mean-field and quantum calculations, where in the latter case we use the time-evolving block decimation algorithm due to Vidal.

Key words: +

PACS:

1 Introduction

Ultracold atoms in optical lattices have recently been at the center of exciting research by both experimental and theoretical physicists alike. In these systems, experimentalists are given an unprecedented amount of control over system parameters, and theorists are able to accurately describe the physics with relatively simple, clean models. However, a full quantum many-body treatment of the problem is computationally challenging due to the exponential growth of the Hilbert space with the system size. There do exist numerous numerical methods, such as quantum Monte Carlo [1] and density matrix renormalization group [2], that can accurately calculate the ground state of the governing quantum Hamiltonian. On the other hand, for systems not exhibiting strong correlations, one can safely employ an appropriate mean-field

theory and describe the many-body system semiclassically, resulting in a much more tractable mathematical problem. Also, before the realization of ultracold atoms, dynamical properties of the many-body lattice problem saw little attention; however, far-from-equilibrium quantum dynamics has recently become a hot topic of research [3,4]. Numerical work in this area has been spurred by the advent of a newly available algorithm for simulating the quantum dynamics of one-dimensional lattice Hamiltonians [5].

In this paper, we study dynamical properties of ultracold bosons on one-dimensional (1D) optical lattices. Our presentation is organized as follows. First, we elucidate the correspondence between the mean-field and quantum many-body theories in the case of the tight-binding approximation on a lattice. Second, we discuss our numerical methods, including an implementation of the time-evolving block decimation algorithm to simulate the quantum dynamics [5]. Finally, we simulate and analyze the time evolution of dark solitons under both the semiclassical and quantum equations of motion and highlight the observed differences between the two theories.

2 Quantum-Mean Field Correspondence

2.1 Mean-Field Theory

The statics and dynamics of a weakly interacting Bose gas at zero temperature in free space, or in the more experimentally relevant geometry of a harmonic trap, are well-described by the Gross-Pitaevskii equation (GP), a.k.a., the nonlinear Schrodinger equation (NLS) [6]. For these simple geometries, even in the quasi-1D regime, such a mean-field approach is appropriate given that there is negligible depletion out of the condensed mode. However, quantum fluctuations cannot be ignored throughout time evolution for certain excited condensate states such as the dark soliton [7,8]. Mean-field theory treatments have been generalized to lattice geometries [9] in which case the lattice soliton solutions of the NLS have been mapped out in detail [10,11]. However, such analysis assumes that the lattice height is sufficiently low so that the gas still exhibits nearly ideal Bose-condensation, i.e., negligible depletion out of the single boson configuration as assumed by the NLS. When using an unperturbed mean-field theory to describe the system, one ideally uses the continuous NLS with an external lattice potential; however, coupled-mode theory can be employed for a shallow lattice [11] or, in the other extreme, a single-band tight-binding approximation can be used for a deep lattice [12].

In the latter case of the tight-binding approximation, assuming 1D from here on, the full condensate wave function $\Phi(x, t)$ is expanded in a basis of localized

condensate wave functions $\phi(x - x_i)$ each centered at site i in the lowest Bloch band of the lattice. That is, $\Phi(x, t) = \sum_i \psi_i(t)\phi(x - x_i)$. It is then assumed that the local condensate wave functions are sufficiently localized in each well, in which case we obtain the well-known discrete nonlinear Schrödinger equation (DNLS):

$$i\hbar\partial_t\psi_k = -J(\psi_{k+1} + \psi_{k-1}) + U|\psi_k|^2\psi_k + \epsilon_k\psi_k, \quad (1)$$

where $\psi_k = \psi_k(t)$ is the dimensionless c-number that weights the localized condensate wave function at the k th lattice site, and ϵ_k is a local external potential different from the lattice potential. The coupling parameter J and the nonlinearity U can be written explicitly in terms of overlap integrals involving the system parameters and the localized condensate wave functions $\phi(x - x_i)$ [12].

2.2 Quantum Many-Body Theory

We now turn to the full quantum many-body description of the problem in the regime of optical lattice depths where the above mean-field tight-binding description is appropriate, and beyond. As was demonstrated by Jaksch *et al.* [13], a system of weakly interacting ultracold bosons loaded in an optical lattice potential is an almost perfect realization of the Bose-Hubbard Hamiltonian (BHH), a model introduced to the condensed matter community almost ten years earlier by Fisher *et al.* [14].

To derive the BHH, we start with the 1D continuous many-body Hamiltonian in second quantization for two-body interactions:

$$\begin{aligned} \hat{H} = & \int dx \hat{\Psi}^\dagger(x) \left[-\frac{\hbar^2}{2m} \frac{\partial^2}{\partial x^2} + V_{\text{ext}}(x) \right] \hat{\Psi}(x) \\ & + \frac{1}{2} \int dx \int dx' \hat{\Psi}^\dagger(x) \hat{\Psi}^\dagger(x') V_{\text{int}}(x - x') \hat{\Psi}(x') \hat{\Psi}(x). \end{aligned} \quad (2)$$

We then expand the bosonic field operator $\hat{\Psi}(x)$, which destroys a particle at position x , in a lowest Bloch band Wannier basis as $\hat{\Psi}(x) = \sum_i \hat{b}_i w(x - x_i)$, where the operator \hat{b}_i is defined to destroy a particle in the localized Wannier wave function $w(x - x_i)$. This step is analogous to expansion of the full condensate wave function in a localized basis when discretizing the continuous NLS to obtain the DNLS. Then, as is done in the derivation of the continuous NLS, we assume the two-body interaction potential to be of the contact form, i.e., $V_{\text{int}}(x - x_i) = g\delta(x - x_i)$, where g is proportional to the s -wave scattering length of the atoms. We also invoke the tight-binding approximation by assuming that the lattice is deep enough to obtain sufficiently localized Wannier functions. This allows us to discard all terms except those involving nearest-neighbor hopping and on-site interactions. After making these assumptions,

we arrive at the familiar BHH:

$$\hat{H} = -J \sum_{i=1}^{M-1} (\hat{b}_{i+1}^\dagger \hat{b}_i + \text{h.c.}) + \frac{U}{2} \sum_{i=1}^M \hat{n}_i (\hat{n}_i - \hat{\mathbb{1}}) + \sum_{i=1}^M \epsilon_i \hat{n}_i, \quad (3)$$

where \hat{b}_i and \hat{b}_i^\dagger are destruction and creation operators at site i that obey the usual bosonic commutation relations, and $\hat{n}_i \equiv \hat{b}_i^\dagger \hat{b}_i$ is the number operator which counts the number of bosons at site i . Equation (3) assumes box boundary conditions on a lattice containing M sites. The coefficients J , U , and ϵ_i can be calculated exactly in terms of the localized single-particle wave functions and other parameters [13]. J is the nearest-neighbor hopping coefficient, U is the on-site interaction energy, and ϵ_i is an external potential. The ratio U/J is an important parameter that determines the relative contribution from each term. For a shallow lattice, the hopping term dominates, whereas for a deep lattice the interaction term dominates. However, we note that U is not completely dependent on the lattice geometry since the s -wave scattering length can be varied independently via a Feshbach resonance.

In deriving the BHH, one makes very similar assumptions to those made when discretizing the continuous NLS on a lattice to obtain the DNLS. Specifically, both derivations invoke a lowest Bloch band tight-binding approximation. However, in the latter case, a single configuration of bosons is assumed from the onset. The full quantum treatment allows for quantum depletion out of the condensate mode and thus can describe the system in the strongly interacting regime.

A general pure state of the full many-body quantum system can be written as a complex linear superposition of states, each with a well-defined number of particles in each Wannier state:

$$|\Psi\rangle = \sum_{n_1, n_2, \dots, n_M=0}^{d-1} c_{n_1 n_2 \dots n_M} |n_1 n_2 \dots n_M\rangle, \quad (4)$$

where n_k is the number of particles at site k . For obvious computational reasons, we truncate the local Hilbert space at local dimension d , i.e., we restrict the occupation of each Wannier state to contain at most $d - 1$ bosons. The Hilbert space containing all pure states of the full many-body system is thus of dimension d^M which becomes prohibitively large for large systems. For example, even for $d = 2$ we can only simulate $M = 12$ or 13 lattice sites on a single PC without further refining the numerical algorithm. We overcome this difficulty with use of the time-evolving block decimation routine which will be discussed in Sec 3.1.

2.3 Discrete Mean-Field Theory From Discrete Quantum Many-Body Theory

Next, we show how the DNLS can be recovered from the BHH. The destruction operator at site k can be evolved in time in the Heisenberg picture according to $i\hbar\partial_t\hat{b}_k = [\hat{b}_k, \hat{H}]$. After computing the commutators, we arrive at

$$i\hbar\partial_t\hat{b}_k = -J(\hat{b}_{k+1} + \hat{b}_{k-1}) + U\hat{b}_k\hat{b}_k^\dagger\hat{b}_k + \epsilon_k\hat{b}_k. \quad (5)$$

We can then take the expectation value of Eq. (5) to obtain an equation of motion for the order parameter $\langle\hat{b}_k\rangle$. The DNLS is recovered exactly if the expectation value is taken with respect to a product of atom-number Glauber coherent states. That is, for full many-body states of the form

$$|\Psi\rangle = \bigotimes_{k=1}^M |z_k\rangle, \text{ where } |z_k\rangle = e^{-\frac{|z_k|^2}{2}} \sum_{n=0}^{\infty} \frac{z_k^n}{\sqrt{n!}} |n\rangle, \quad (6)$$

we obtain the DNLS for the equation of motion governing the coherent state amplitude $z_k = \langle\hat{b}_k\rangle$:

$$i\hbar\partial_t z_k = -J(z_{k+1} + z_{k-1}) + U|z_k|^2 z_k + \epsilon_k z_k. \quad (7)$$

As discussed in Sec. 2.2, for numerical calculations we must truncate the local Hilbert space to a finite dimension d , in which case the on-site coherent states of Eq. (6) become *truncated* coherent states:

$$|\Psi\rangle = \bigotimes_{k=1}^M |z_k\rangle, \text{ where } |z_k\rangle = \mathcal{N}_d e^{-\frac{|z_k|^2}{2}} \sum_{n=0}^{d-1} \frac{z_k^n}{\sqrt{n!}} |n\rangle, \quad (8)$$

and \mathcal{N}_d is a normalization factor.

The coherent states of Eq. (6) are known to well-describe the ground state of the BHH for $J \gg U$ in the limit of an infinite number of sites M and particles N at fixed filling N/M [15]. It is in this regime that quantum depletion can be safely neglected and Eq. (7) is an accurate description of the system. However, the lattice must still be deep enough so that the single-band tight-binding approximation is still valid. In Sec. 4, we use the truncated coherent states of Eq. (8) to create nonequilibrium initial quantum states in the BHH that are analogs to the dark soliton solutions of the DNLS.

3 Numerical Methods

3.1 Time-Evolving Block Decimation Algorithm

The time-evolving block decimation (TEBD) algorithm was first introduced in 2003-2004 by Vidal [16,5] in the context of quantum computation. Soon thereafter, Daley *et al.* [17] and White and Feiguin [18] translated the algorithm into more the familiar density matrix renormalization group (DMRG) language and showed that TEBD is equivalent to a time-*adaptive* DMRG routine. Here, we summarize our implementation of TEBD as applied to the BHH.

3.1.1 The Vidal Decomposition

The Vidal prescription is to first rewrite the coefficients in Eq. (4) as a product of M tensors $\{\Gamma^{[\ell]}\}$ and $M - 1$ vectors $\{\lambda^{[\ell]}\}$:

$$c_{n_1 n_2 \dots n_M} = \sum_{\alpha_1, \dots, \alpha_{M-1}=1}^{\chi} \Gamma_{\alpha_1}^{[1]n_1} \lambda_{\alpha_1}^{[1]} \Gamma_{\alpha_1 \alpha_2}^{[2]n_2} \lambda_{\alpha_2}^{[2]} \Gamma_{\alpha_2 \alpha_3}^{[3]n_3} \dots \Gamma_{\alpha_{M-1}}^{[M]n_M}. \quad (9)$$

There does exist a procedure for determination of the Γ 's and λ 's given known coefficients of an arbitrary state; however, this is not generally useful because one does not typically have access to each component of the d^M -dimensional vector $|\Psi\rangle$. This procedure would require a Schmidt decomposition (SD) at every bipartite splitting of the lattice, where $\chi \leq d^{\lfloor M/2 \rfloor}$ is the number of Schmidt vectors retained at each splitting. The Schmidt number χ_S , i.e., the number of Schmidt basis sets required for an exact representation of the state at each cut, is naturally a measure of global entanglement between the lattice sites [16,19]. The decomposition (9) is thus appropriate when $|\Psi\rangle$ is only slightly entangled according to the Schmidt number, in which case it is computationally feasible to take $\chi \approx \chi_S$.

3.1.2 Two-Site Operation

One of the reasons why this decomposition is useful is that it allows for efficient application of two-site unitary operations. Let us consider a two-site unitary operation $\hat{V} = \sum V_{n'_\ell n'_{\ell+1}}^{n_\ell n_{\ell+1}} |n_\ell n_{\ell+1}\rangle \langle n'_\ell n'_{\ell+1}|$ acting on sites ℓ and $\ell + 1$. First, we write $|\Psi\rangle$ in terms of Schmidt vectors for the subsystems $[1 \dots \ell - 1]$ and

$[\ell + 2 \cdots M]$:

$$\begin{aligned}
|\Psi\rangle &= \sum_{\alpha_{\ell-1}, \alpha_{\ell}, \alpha_{\ell+1}; n_{\ell}, n_{\ell+1}} \lambda_{\alpha_{\ell-1}}^{[\ell-1]} \Gamma_{\alpha_{\ell-1} \alpha_{\ell}}^{[\ell] n_{\ell}} \lambda_{\alpha_{\ell}}^{[\ell]} \Gamma_{\alpha_{\ell} \alpha_{\ell+1}}^{[\ell+1] n_{\ell+1}} |\Phi_{\alpha_{\ell-1}}^{[1 \cdots \ell-1]}\rangle \otimes |n_{\ell} n_{\ell+1}\rangle \otimes |\Phi_{\alpha_{\ell+1}}^{[\ell+2 \cdots M]}\rangle \\
&= \sum_{\alpha_{\ell-1}, \alpha_{\ell+1}; n_{\ell}, n_{\ell+1}} \Theta_{\alpha_{\ell-1} \alpha_{\ell+1}}^{n_{\ell} n_{\ell+1}} |\Phi_{\alpha_{\ell-1}}^{[1 \cdots \ell-1]}\rangle \otimes |n_{\ell} n_{\ell+1}\rangle \otimes |\Phi_{\alpha_{\ell+1}}^{[\ell+2 \cdots M]}\rangle \quad (10)
\end{aligned}$$

by invoking Eqs. (13) and (14) of [16], where

$$\Theta_{\alpha_{\ell-1} \alpha_{\ell+1}}^{n_{\ell} n_{\ell+1}} \equiv \sum_{\alpha_{\ell}} \lambda_{\alpha_{\ell-1}}^{[\ell-1]} \Gamma_{\alpha_{\ell-1} \alpha_{\ell}}^{[\ell] n_{\ell}} \lambda_{\alpha_{\ell}}^{[\ell]} \Gamma_{\alpha_{\ell} \alpha_{\ell+1}}^{[\ell+1] n_{\ell+1}} \lambda_{\alpha_{\ell+1}}^{[\ell+1]} \quad (11)$$

and $\alpha_{\ell} \in \{1, 2, \dots, \chi\}$. Note that this definition of the tensor Θ differs from an analogous construct in [16] which is also denoted Θ in that work. We are up to this point assuming that we know the decomposition (9) of $|\Psi\rangle$, and hence we also know all elements of Θ . However, by writing $|\Psi\rangle$ in the form of Eq. (10) we can easily write the updated state after the application of \hat{V} as

$$\hat{V}|\Psi\rangle = \sum_{\alpha_{\ell-1}, \alpha_{\ell+1}; n_{\ell}, n_{\ell+1}} \tilde{\Theta}_{\alpha_{\ell-1} \alpha_{\ell+1}}^{n_{\ell} n_{\ell+1}} |\Phi_{\alpha_{\ell-1}}^{[1 \cdots \ell-1]}\rangle \otimes |n_{\ell} n_{\ell+1}\rangle \otimes |\Phi_{\alpha_{\ell+1}}^{[\ell+2 \cdots M]}\rangle, \quad (12)$$

where $\tilde{\Theta}$ can be written in terms of the updated tensors $\tilde{\Gamma}^{[\ell]}$ and $\tilde{\Gamma}^{[\ell+1]}$ and the updated vector $\tilde{\lambda}^{[\ell]}$:

$$\tilde{\Theta}_{\alpha_{\ell-1} \alpha_{\ell+1}}^{n_{\ell} n_{\ell+1}} = \sum_{n'_{\ell}, n'_{\ell+1}} V_{n'_{\ell} n'_{\ell+1}}^{n_{\ell} n_{\ell+1}} \Theta_{\alpha_{\ell-1} \alpha_{\ell+1}}^{n'_{\ell} n'_{\ell+1}} = \sum_{\tilde{\alpha}_{\ell}} \lambda_{\alpha_{\ell-1}}^{[\ell-1]} \tilde{\Gamma}_{\alpha_{\ell-1} \tilde{\alpha}_{\ell}}^{[\ell] n_{\ell}} \tilde{\lambda}_{\tilde{\alpha}_{\ell}}^{[\ell]} \tilde{\Gamma}_{\tilde{\alpha}_{\ell} \alpha_{\ell+1}}^{[\ell+1] n_{\ell+1}} \lambda_{\alpha_{\ell+1}}^{[\ell+1]}. \quad (13)$$

In practice, a given two-site operation is performed as follows: (1) form Θ from current Γ s and λ s [Eq. (11)]; (2) update Θ by applying \hat{V} to obtain $\tilde{\Theta}$ [Eq. (13)]; (3) reshape $\tilde{\Theta}$ from a 4-tensor to a $(\chi d) \times (\chi d)$ matrix; (4) perform a singular value decomposition (SVD) on this matrix retaining only the largest χ singular values $\tilde{\lambda}_{\tilde{\alpha}_{\ell}}^{[\ell]}$; and (5) divide out the previous values of $\lambda^{[\ell-1]}$ and $\lambda^{[\ell+1]}$ in order to compute $\tilde{\Gamma}^{[\ell]}$ and $\tilde{\Gamma}^{[\ell+1]}$ from the matrix elements obtained via the SVD. The most expensive computational steps are (1), the formation of Θ , and (2), the update of Θ after the application of \hat{V} . The former requires $\mathcal{O}(d^2 \chi^3)$ elementary operations, whereas the latter requires $\mathcal{O}(d^4 \chi^2)$ elementary operations; hence, our overall two-site operation scales as $\mathcal{O}[\max(d^2 \chi^3, d^4 \chi^2)]$.

3.1.3 Real Time Evolution

The BHH is a sum of one- and two-site operations, but the terms multiplying J in Eq. (3) do not all commute, so the time evolution operator $e^{-i\hat{H}t/\hbar}$ does not directly factor into a product of one- and two-site unitary operations. However, because the BHH only links nearest neighbors, we write $\hat{H} = \hat{H}_{\text{odd}} + \hat{H}_{\text{even}}$,

where

$$\hat{H}_{\text{odd}} = -J \sum_{i \text{ odd}} (\hat{b}_{i+1}^\dagger \hat{b}_i + \text{h.c.}) + \sum_{i \text{ odd}} \left[\frac{U}{2} \hat{n}_i (\hat{n}_i - \hat{1}) + \epsilon_i \hat{n}_i \right] \quad \text{and} \quad (14)$$

$$\hat{H}_{\text{even}} = -J \sum_{i \text{ even}} (\hat{b}_{i+1}^\dagger \hat{b}_i + \text{h.c.}) + \sum_{i \text{ even}} \left[\frac{U}{2} \hat{n}_i (\hat{n}_i - \hat{1}) + \epsilon_i \hat{n}_i \right]. \quad (15)$$

Each term *within* both \hat{H}_{odd} and \hat{H}_{even} commute even though $[\hat{H}_{\text{odd}}, \hat{H}_{\text{even}}] \neq 0$. It is then convenient to utilize a Suzuki-Trotter approximation of the time evolution operator for small time steps δt . Specifically, we employ the second-order expansion: $e^{-i\hat{H}\delta t/\hbar} \approx e^{-i\hat{H}_{\text{odd}}\delta t/2\hbar} e^{-i\hat{H}_{\text{even}}\delta t/\hbar} e^{-i\hat{H}_{\text{odd}}\delta t/2\hbar}$, where each exponential factor can be factored into a product of two-site unitaries. Even though the terms involving \hat{n} are one-site operations, we still treat them as two-site operations by appropriate tensor products with the identity operator. In practice, we build d^2 -dimensional matrix representations of \hat{H} for each lattice link and diagonalize these matrices to obtain matrix representations of the two-site unitary operators. Then, in conjunction with the Suzuki-Trotter expansion, we employ the two-site operation procedure outlined in Sec. 3.1.2 on an initial decomposed configuration $|\Psi\rangle$ $\mathcal{O}(M)$ times for each of $t_f/\delta t$ total time steps, updating the decomposition at each step. It is straightforward to calculate single-site observables, e.g., the expectation value of the number operator $\langle \hat{n}_k \rangle$, and two-site observables, e.g., the one-body density matrix $\langle \hat{b}_i^\dagger \hat{b}_j \rangle$, by using the partial trace to calculate the reduced density matrix of the subsystem of interest. For example, to calculate $\langle \hat{b}_i^\dagger \hat{b}_j \rangle$, we first compute $\hat{\rho}_{ij} = \text{tr}_{k \neq i,j} |\Psi\rangle \langle \Psi|$ using Eq. (9) for $|\Psi\rangle$ and then use $\langle \hat{b}_i^\dagger \hat{b}_j \rangle = \text{tr}(\hat{b}_i^\dagger \otimes \hat{b}_j \hat{\rho}_{ij})$. Overall, our implementation of the TEBD algorithm scales as $\mathcal{O}[M \frac{t_f}{\delta t} \max(d^2 \chi^3, d^4 \chi^2)]$.

3.1.4 Sources of Error and Convergence Properties

The TEBD algorithm makes two important approximations: (1) the retention of only the χ most heavily weighted basis sets during a given two-site operation (see Sec. 3.1.2), and (2) the Suzuki-Trotter representation of the time evolution operator (see Sec. 3.1.3). For the latter case, we find that for the results presented in Sec. 4 it is sufficient to use time steps of size $\delta t = 0.01 \hbar/J$ to obtain converged results. The former approximation is more subtle as its accuracy is directly related to the amount of entanglement present in the system. Specifically, in Sec. 4, we time evolve mean-field initial states [see Eq. (8)] for which $\chi = 1$ is sufficient for exact representation; however, unitary time evolution increases entanglement between sites. To ensure that our choice of χ is sufficient, we run equivalent simulations with increasing values of χ and look for convergence of calculated observables, e.g., average local number $\langle \hat{n}_k \rangle$. It is important to point out that, owing to the local nature of the expansion (9), accurate calculation of nonlocal observables, e.g., off-diagonal elements of the single-particle density matrix, converge more slowly with respect to χ . For the

observables and time scales presented in Sec. 4, our results are converged for the specified values of $\chi = 45, 50$. We also note that the fidelity of truncation at χ eigenvalues can be quantified by the sum of the non-retained eigenvalues after application of a two-site operation. This quantity can be interpreted as a measure of the amount of entanglement generated by the two-site operation. Typically, for a single two-site unitary, we find this truncation error to be less than or on the order of 10^{-6} .

3.2 Constrained Imaginary Time Relaxation in DNLS

3.2.1 Fundamental Dark Soliton Solutions

In Sec. 4, we use the TEBD routine to simulate the quantum evolution of the dark soliton solutions of the DNLS by using truncated coherent states as initial configurations. This requires knowledge of the set of coherent state amplitudes $\{z_k\}$ corresponding to a discrete dark soliton. Using a standard Crank-Nicolson scheme for the time-stepping procedure, we calculate the standing dark soliton solution of the DNLS by performing constrained imaginary time relaxation on Eq. (7) with $\epsilon_k = 0$. Specifically, we take an initial condition of form $z_k = mx_k$ where x_k is the position of the k th site and $x = 0$ is the center of the lattice and normalize the solution to $N_{\text{DNLS}} = \sum_{k=1}^M |z_k|^2$ at each step of imaginary time. The stationarity of the solution is tested by subsequent evolution in real time.

3.2.2 Density and Phase Engineering of Gray Solitons

We also consider the case of two solitons moving toward one another at finite velocity. These initial conditions are obtained via the methods of density and phase engineering for soliton creation [20] as applied to the DNLS. We first perform imaginary time relaxation on a uniform initial condition with an external potential of the form

$$\epsilon_k = V_0 \left\{ \exp \left[-\frac{(x_k + \xi)^2}{2\sigma_\epsilon^2} \right] + \exp \left[-\frac{(x_k - \xi)^2}{2\sigma_\epsilon^2} \right] \right\} \quad (16)$$

to dig two density notches each centered at distance ξ from the center of the lattice. Next, we imprint an instantaneous phase of the form

$$\theta_k = \Delta\theta \left\{ -\frac{1}{2} \tanh \left[\frac{2(x_k + \xi)}{\sigma_\theta} \right] + \frac{1}{2} \tanh \left[\frac{2(x_k - \xi)}{\sigma_\theta} \right] + 1 \right\} \quad (17)$$

which gives the solitons equal-and-opposite initial velocities toward the center of the lattice. Phonon generation is minimized by appropriately tuning the

width σ_θ of the phase profiles to the soliton depth as determined by V_0 in the density engineering stage.

4 Time Evolution of Quantum Solitons

With an initial DNLS configuration $\{z_k(0)\}$ obtained either via the procedure outlined in Sec. 3.2.1 for a single standing soliton or the procedure outlined in Sec. 3.2.2 for two colliding solitons, we then build a product of truncated coherent states according to Eq. (8) for input into the TEBD quantum simulation routine. The Vidal decomposition (9) of a product state $|\Psi\rangle = \otimes_{k=1}^M \left(\sum_{n_k=0}^{d-1} c_{n_k}^{(k)} |n_k\rangle \right)$ is trivial to compute:

$$\lambda_{\alpha_\ell}^{[\ell]} = \delta_{\alpha_\ell,1} \quad \text{and} \quad \Gamma_{\alpha_{\ell-1}\alpha_\ell}^{[\ell]n_\ell} = c_{n_\ell}^{(\ell)} \delta_{\alpha_{\ell-1},1} \delta_{\alpha_\ell,1}, \quad (18)$$

where for the case of truncated coherent states $c_n^{(k)} = \mathcal{N}_d e^{-|z_k|^2/2} \frac{z_k^n}{\sqrt{n!}}$.

An extensive discussion of results obtained using the above methodology to create nonequilibrium dark soliton initial states in the BHH is presented in Refs. [21,22]. We will summarize those results here. Being direct analogs of mean-field solitons, the initial conditions analyzed below do not conserve total particle number, although quantum evolution does conserve total *average* particle number. That is, in this section, we consider the quantum many-body evolution of mean-field-like solitons and refer to these structures as *quantum solitons*. However, we stress that neither the discrete mean-field theory (DNLS) nor the corresponding quantum theory (BHH) are integrable systems, so these are not solitons in the mathematically rigorous sense. It is possible to density and phase engineer dark soliton states directly in the BHH that are eigenfunctions of the total number operator. In Ref. [22], we use a number-conserving version of the TEBD routine to generate and analyze the quantum dynamics of such states. Although some observables behave differently in this case, the conclusions reached are generally the same.

4.1 Standing Solitons

The DNLS assumes a single configuration of bosons, i.e., bosons are only allowed to occupy one single-particle orbital. However, for an M mode system, a full quantum treatment will permit bosons to occupy any of the M permissible modes. For the system sizes accessible to explore with the TEBD routine, a standing soliton initial DNLS configuration exhibits a finite lifetime due to quantum effects indescribable by mean-field theory. Most notably, quantum evolution causes significant quantum depletion out of the initial dark soliton

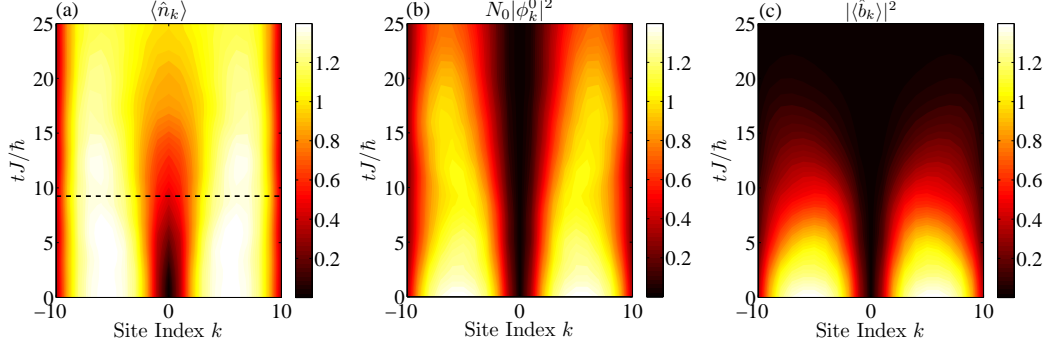


Fig. 1. *Density measures for a standing quantum soliton.* Quantum evolution of (a) average particle number, (b) condensate wave function [23], and (c) order parameter versus position and time for a standing DNLS dark soliton initial configuration. The dashed line in (a) indicates the $1/e$ decay time of the order parameter norm N_b .

configuration into higher order orbitals which fill in the soliton density notch, where as discussed in [21], the natural orbitals of the system are defined as the eigenfunctions of the one-body density matrix $\langle \hat{b}_i^\dagger \hat{b}_j \rangle$ [23]. We find that the soliton lifetime is closely correlated to the the growth in quantum effects such as a decay in the order parameter norm $N_b = \sum_{k=1}^M |\langle \hat{b}_k \rangle|^2$ and growth in the generalized entropy $Q = \frac{d}{d-1} \left[1 - \frac{1}{M} \sum_{k=1}^M \text{tr}(\hat{\rho}_k^2) \right]$. Shown in Fig. 1 is the evolution of density measures of a quantum soliton with parameters $\nu U/J = 0.35$, $\nu = 1$, $M = 21$, $d = 7$, $\chi = 45$, where $\nu = N_{\text{DNLS}}/M$ is approximately equal to the average filling.

4.2 Soliton-Soliton Collisions

In Fig. 2, we display the quantum evolution of two colliding dark solitons where the initial conditions were obtained by density and phase engineering in the DNLS as summarized in Sec. 3.2.2. Here, if the decoherence time, as measured by the decay time of the order parameter norm, occurs before or near the collision time, then there is a loss in elasticity of the soliton collision. For a fixed value of the effective nonlinearity $\nu U/J$, we can independently tune the decoherence time by changing the filling ν without altering the initial density-phase profile of the solitons. In Fig. 2, we depict this effect in three separate simulations with parameters $\nu U/J = 0.35$, $M = 31$, $\chi = 50$, $V_0/J = 0.4$, $\sigma_\epsilon/a = 1$, $\Delta\theta = 0.3\pi$, $\sigma_\theta/a = 2$, $\xi/a = 6$ at filling factors $\nu = 1, 0.5, 0.1$, where a is the lattice constant.

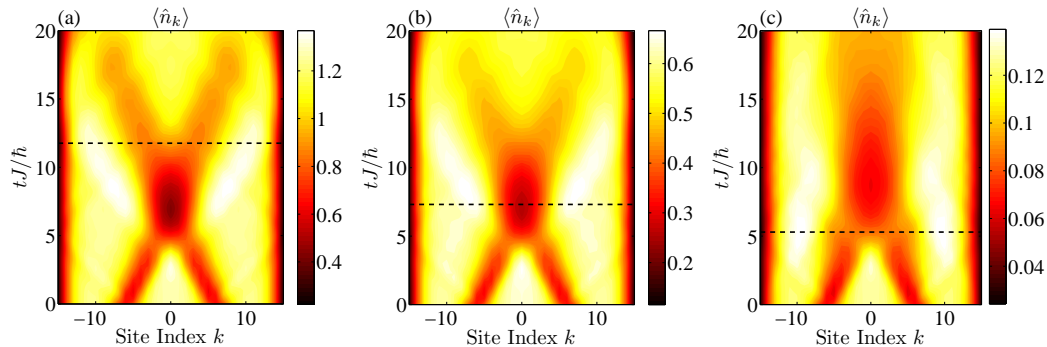


Fig. 2. *Quantum soliton collisions and decoherence-induced inelasticity.* Average particle number for two colliding quantum solitons at filling factors (a) $\nu = 1$, (b) $\nu = 0.5$, and (c) $\nu = 0.1$. The collision elasticity is decreased when the decoherence time (dashed lines) occurs at or before the time of collision.

5 Conclusion

In conclusion, we have summarized the derivations of the DNLS both from the continuous mean field and from the continuous quantum field. In both cases, we invoke a single-band tight-binding approximation; however, the latter derivation from the quantum many-body perspective is more insightful as it is based on single-particle physics with single-orbital occupation not assumed until the end. Using Vidal's TEBD routine to propagate dark soliton DNLS configurations forward in time according to the BHH, we have shown that quantum fluctuations give dark solitons a finite lifetime and induce an inelasticity in soliton-soliton collisions. For a more extensive analysis of these results, we refer the reader to Refs. [21,22].

We thank Charles Clark, Ippei Danshita, and Jamie Williams for useful discussions. This material is based upon work supported by the National Science Foundation under Grant No. PHY-0547845, as part of the NSF CAREER program.

References

- [1] W. M. C. Foulkes, L. Mitas, R. J. Needs, G. Rajagopal, Quantum Monte Carlo simulations of solids, *Rev. Mod. Phys.* 73 (2001) 33-83.
- [2] U. Schollwöck, The density-matrix renormalization group, *Rev. Mod. Phys.* 77 (2005) 259-315.

- [3] T. Kinoshita, T. Wenger, D. S. Weiss, A quantum Newton's cradle, *Nature* 440 (2006) 900-903.
- [4] C. Kollath, A. M. Läuchli, E. Altman, Quench Dynamics and Nonequilibrium Phase Diagram of the Bose-Hubbard Model, *Phys. Rev. Lett.* 98 (2007) 180601.
- [5] G. Vidal, Efficient Simulation of One-Dimensional Quantum Many-Body Systems, *Phys. Rev. Lett.* 93 (2004) 040502.
- [6] F. Dalfovo, S. Giorgini, L. P. Pitaevskii, S. Stringari, Theory of Bose-Einstein condensation in trapped gases, *Rev. Mod. Phys.* 71 (1999) 463-512.
- [7] J. Dziarmaga, Z. P. Karkuszewski, K. Sacha, Quantum depletion of an excited condensate, *Phys. Rev. A* 66 (2002) 043615.
- [8] J. Dziarmaga, Z. P. Karkuszewski, K. Sacha, Images of the dark soliton in a depleted condensate, *J. Phys. B* 36 (2003) 1217.
- [9] J. C. Bronski, L. D. Carr, B. Deconinck, J. N. Kutz, Bose-Einstein Condensates in Standing Waves: The Cubic Nonlinear Schrödinger Equation with a Periodic Potential, *Phys. Rev. Lett.* 86 (2001) 1402.
- [10] P. J. Y. Louis, E. A. Ostrovskaya, C. M. Savage, Y. S. Kivshar, Bose-Einstein condensates in optical lattices: Band-gap structure and solitons, *Phys. Rev. A* 67 (2003) 013602.
- [11] N. K. Efremidis, D. N. Christodoulides, Lattice solitons in Bose-Einstein condensates, *Phys. Rev. A* 67 (2003) 063608.
- [12] A. Trombettoni, A. Smerzi, Discrete Solitons and Breathers with Dilute Bose-Einstein Condensates, *Phys. Rev. Lett.* 86 (2001) 2353-2356.
- [13] D. Jaksch *et al.*, Cold Bosonic Atoms in Optical Lattices, *Phys. Rev. Lett.* 81 (1998) 3108-3111.
- [14] M. P. A. Fisher, P. B. Weichman, G. Grinstein, D. S. Fisher, Boson localization and the superfluid-insulator transition, *Phys. Rev. B* 40 (1989) 546-570.
- [15] W. Zwerger, Mott-Hubbard transition of cold atoms in optical lattices, *J. Opt. B: Quantum Semiclassical Opt.* 5 (2003) S9-S16.
- [16] G. Vidal, Efficient Classical Simulation of Slightly Entangled Quantum Computations, *Phys. Rev. Lett.* 91 (2003) 147902.
- [17] A. J. Daley, C. Kollath, U. Schollwöck, G. Vidal, Time-dependent density-matrix renormalization-group using adaptive effective Hilbert spaces, *J. Stat. Mech.* (2004) P04005.
- [18] S. R. White and A. E. Feiguin, Real-Time Evolution Using the Density Matrix Renormalization Group, *Phys. Rev. Lett.* 93 (2004) 076401.
- [19] M. A. Nielsen and I. L. Chuang, *Quantum Computation and Quantum Information*, Cambridge University Press, Cambridge, 2000.

- [20] L. D. Carr, J. Brand, S. Burger, A. Sanpera, Dark-soliton creation in Bose-Einstein condensates, *Phys. Rev. A* 63 (2001) 051601.
- [21] R. V. Mishmash, L. D. Carr, Quantum Entangled Dark Solitons Formed by Ultracold Atoms in Optical Lattices, *Phys. Rev. Lett.*, under review, arXiv:0710.0045v2 [cond-mat.mes-hall] (2007).
- [22] R. V. Mishmash, I. Danshita, C. W. Clark, and L. D. Carr, Quantum Many-Body Dynamics of Dark Solitons in Optical Lattices, *Phys. Rev. A*, to be submitted (2008).
- [23] O. Penrose, L. Onsager, Bose-Einstein Condensation and Liquid Helium, *Phys. Rev.* 104 (1956) 576-584.